

Discovery of Phosphoric Acid Mono-{2-[(*E/Z*)-4-(3,3-dimethyl-butyrylamino)-3,5-difluoro-benzoylimino]-thiazol-3-ylmethyl} Ester (Lu AA47070): A Phosphonooxymethylene Prodrug of a Potent and Selective hA_{2A} Receptor Antagonist

Anette G. Sams,^{*,†,‡} Gitte K. Mikkelsen,[‡] Mogens Larsen,[‡] Morten Langgård,^{||} Mark E. Howells,^{⊥,§} Tenna J. Schröder,[¶] Lise T. Brennum,[∇] Lars Torup,[∇] Erling B. Jørgensen,[◆] Christoffer Bundgaard,[#] Mads Kreilgård,[#] and Benny Bang-Andersen[‡]

[‡]Medicinal Chemistry Research, Lundbeck Research Denmark, H. Lundbeck A/S, Ottiliavej 9, DK-2500 Copenhagen Valby, Denmark,

^{||}Computational Chemistry, Lundbeck Research Denmark, H. Lundbeck A/S, Ottiliavej 9, DK-2500 Copenhagen Valby, Denmark, [⊥]Process Research, H. Lundbeck A/S, Ottiliavej 9, DK-2500 Copenhagen Valby, Denmark, [¶]Molecular Pharmacology, Lundbeck Research Denmark, H. Lundbeck A/S, Ottiliavej 9, DK-2500 Copenhagen Valby, Denmark, [∇]In vivo Neuropharmacology, Lundbeck Research Denmark, H. Lundbeck A/S, Ottiliavej 9, DK-2500 Copenhagen Valby, Denmark, [◆]Preformulation, Lundbeck Research Denmark, H. Lundbeck A/S, Ottiliavej 9, DK-2500 Copenhagen Valby, Denmark, and [#]Discovery ADME, Lundbeck Research Denmark, H. Lundbeck A/S, Ottiliavej 9, DK-2500 Copenhagen Valby, Denmark. [‡]Current address: LEO Pharma A/S, Industriparken 55, DK-2750 Ballerup, Denmark.

[§]Current address: Novozymes A/S, Hallas Alle 1, DK-4400 Kalundborg, Denmark.

Received July 12, 2010

The discovery and structure–activity relationship of a series of hA_{2A} receptor antagonists is described. Compound **28** was selected from the series as a potent and selective compound and was shown to be efficacious in an *in vivo* model of Parkinson's disease. It had acceptable ADME properties; however, the low intrinsic solubility of this compound was limiting for its developability, because the oral bioavailability from dosing in suspension was significantly lower than the oral bioavailability from solution dosage. As a consequence, prodrugs of **28** were prepared with dramatically increased aqueous solubility. The prodrugs efficiently delivered **28** into systemic circulation, with no detectable levels of prodrug in plasma samples. From this investigation, we selected **32** (Lu AA47070), a phosphonooxymethylene prodrug of **28**, as a drug candidate.

Introduction

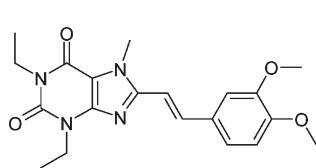
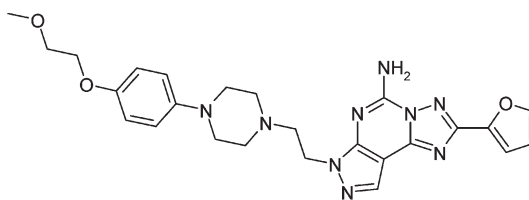
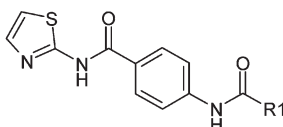
Adenosine (A)^a is an important neuromodulator, and its action is mediated via a family of four specific G-protein coupled receptors (GPCRs). Four adenosine receptors have been cloned and characterized, A₁, A_{2A}, A_{2B}, and A₃.¹ The receptors differ in their affinity toward adenosine, as well as in their downstream signaling pathways. Activation of the A_{2A} and A_{2B} receptor subtypes leads to the activation of adenylyl cyclase, resulting in the formation of cAMP, whereas adenosine A₁ and adenosine A₃ receptors are inhibitory toward cAMP production.² In the central nervous system (CNS), the adenosine A_{2A} receptor is highly expressed in the striatum,

nucleus accumbens, and olfactory tubercle in humans, while low levels are found in other brain areas. The adenosine A_{2A} receptor is coexpressed with dopamine D₂ receptors in striatum and is involved in the regulation of functional activity of dopamine D₂ receptors, and heterodimerization of A_{2A} and D₂ receptor subtypes inhibit dopamine D₂ receptor function.^{3,4} Adenosine A_{2A} receptors have also been shown to modulate the release of GABA in the striatum. By reducing the GABA output, adenosine A_{2A} receptor antagonism helps counteract striatal dopamine depletion and restore normal function in the basal ganglia. Therefore, A_{2A} receptor antagonists may have clinical utility in the treatment of Parkinson's disease, a progressively debilitating motor disorder arising from the degeneration of dopaminergic neurons in the nigrostriatal pathway.³

The identification and development of potent and selective human (h) A_{2A} receptor antagonists has been intensively pursued by pharmaceutical companies, as well as academia, for several years and has recently been reviewed.^{5–7} (For recent examples, see refs 8–21) From this effort, a number of compounds have progressed into clinical trials. Currently, **1** (KW-6002)²² has progressed to phase 3 trials for Parkinson's disease, and **2** (SCH-420814)²³ is in phase 2 trials for Parkinson's disease (Chart 1). Generally, hA_{2A} receptor antagonists are structurally classified into xanthine-like structures, as exemplified by **1**, and non-xanthine-like structures. Members of the latter classification comprise a structurally diverse group of chemotypes. Following the structural elucidation of the hA_{2A} receptor,²⁴ structure-based approaches to the identification

*Corresponding author. Phone: +45 44945888. Fax: +45 72263320. E-mail: anette.sams@leo-pharma.com.

^a Abbreviations: A, adenosine; GPCR, G-protein coupled receptor; CNS, central nervous system; cAMP, cyclic adenosine monophosphate; GABA, γ -amino butyric acid; PD, pharmacodynamics; ADME, absorption–distribution–metabolism–excretion; PK, pharmacokinetics; SD, standard deviation; P-gp, permeability glycoprotein; po, *per os* (orally); iv, intravenous; BSA, bovine serum albumin; CHO, chinese hamster ovary; HEK, human kidney embryonic; HMBC, heteronuclear multiple bond correlation; HPLC, high-pressure MS, liquid chroma/MS, liquid chromatography/mass spectrometry; UV, ultraviolet; EDC, *N*-ethyl-*N'*-dimethylaminopropyl-carbodiimide hydrochloride; HOBt, 1-hydroxy-benzotriazole; HATU, 2-(1*H*-7-azabenzotriazol-1-yl)-1,1,3,3-tetramethyluronium hexafluorophosphate; DIPEA, diisopropyl-ethylamine; NBS, *N*-bromosuccinimide; TFA, trifluoroacetic acid; DCM, dichloromethane; 1,2-DCE, 1,2-dichloroethane; DMF, dimethylformamide; DMAc, dimethylacetamide; THF, tetrahydrofuran; dppf, 1,1'-bis(diphenylphosphino)ferrocene; Boc, *N*-tert-butoxycarbonyl.

Chart 1. Structures of hA_{2A} Receptor Antagonists**1:** Istradefylline (KW-6002)**2:** Preladenant (SCH420814)**3:** R¹ = *o*-tolyl**4:** R¹ = *n*-butyl

of new chemotypes of hA_{2A} receptor ligands have been reported.^{25,26} Common for many hA_{2A} receptor antagonists are their planar, aromatic structures, and as a consequence thereof, many compounds are hampered by very low aqueous solubility.

Herein we describe the discovery of a novel structural class of hA_{2A} receptor antagonists. From this series, **28** was selected as a highly selective compound with acceptable pharmacokinetic (PK) properties and with effect in an *in vivo* model of PD. However, the aqueous solubility of **28** was limiting for the potential of this compound to become a drug. Consequently, **28** was derivatized as water-soluble prodrugs, which improved the aqueous solubility by several thousand fold compared with **28**. The prodrugs were fully converted to **28** *in vivo*, with no detectable prodrug in systemic circulation. From these prodrugs, we selected the phosphonoxymethylene derivative **32** (Lu AA47070) for clinical development based on its superior properties.

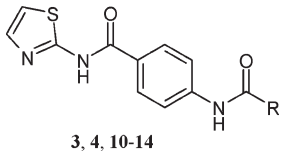
Results and Discussion

In our efforts to identify novel A_{2A} receptor antagonists, a high-throughput screening campaign of a collection of approximately 200 000 compounds was conducted, using a binding assay with [³H]ZM241385 as radio ligand and membranes from a commercially available cell line stably expressing rat A_{2A} receptors (MCL-511, PerkinElmer). Among the hits were two 4-carboxamido-*N*-thiazol-2-yl-benzamides (compounds **3** and **4**), differing only at the 4-carboxamido substituent as shown in Chart 1. These compounds represented a novel structural class of A_{2A} receptor ligands. Initial *in vitro* profiling of these hits for selectivity toward the hA₁ receptor and *in vitro* ADME properties revealed few differences in their profiles as summarized in Table 1. The affinities of **3** and **4** to the hA_{2A} receptor were equipotent, with *K_i* values around 200 nM. Also, the compounds did not differentiate with respect to their selectivity toward the hA₁ receptor determined as displacement of the radioligand [³H]DPCPX in membranes from Chinese hamster ovary (CHO) cells stably expressing hA₁ receptors. Thus, **3** and **4** showed inhibition of [³H]DPCPX binding of 47% and 69% at 10 μM test

concentration, respectively, indicating *K_i*'s > 2000 nM for hA₁ receptors. For comparison, **1** had a *K_i* for hA_{2A} receptors of 72 nM and a *K_i* of 3000 nM for hA₁ receptors, whereas **2** had a *K_i* of 5 nM for hA_{2A} receptors and inhibited [³H]DPCPX binding by 30% at 2000 nM, indicating a *K_i* > 1000 nM for hA₁ receptors.

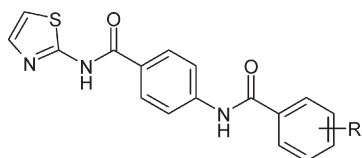
Both hit compounds **3** and **4** showed acceptable *in vitro* ADME properties, that is, incubating **3** and **4** with human and rat liver microsomes resulted in **3** showing good stability (human *Cl_{int}* = 0.5 L/min; rat *Cl_{int}* = 5 mL/min), while **4** showed moderate stability (human *Cl_{int}* = 2.3 L/min; rat *Cl_{int}* = 54 mL/min). For comparison, the human and rat liver blood flow is 1.4 L/min and 20 mL/min, respectively. The difference in stability must derive from the amide substituents in the compounds. Furthermore, both compounds were highly membrane permeable in the Caco-2 cell assay, with no indication of active efflux transport. In a panel screen of CYP P450 enzymes, the compounds were differentiated. Thus, while **3** was a reasonably potent inhibitor of CYP3A4 (*IC₅₀* = 1.4 μM), compound **4** displayed no inhibition of any of the CYP enzymes (*IC₅₀* > 40 μM).

Although none of the hit compounds had an overall optimal preliminary *in vitro* profile, the data suggested that the compounds could be optimized. Since the hits only differed at the carboxamide substituent, we initially explored the requirements and limitations of this substituent. With **3** as a starting point, the series of analogues shown in Figure 1 were prepared. However, none of these compounds showed any improvements over **3**, displaying affinities (*K_i*) for the hA_{2A} receptor in the range of 300–500 nM. Hence, **3** was not further pursued (see the Supporting Information for details). We then turned our attention toward hit compound **4**, which was first examined by shortening the amide alkyl chain (Table 1). Thus, replacing *n*-butyl with *n*-propyl gave compound **10** having a very similar profile to **4** in terms of hA_{2A} receptor affinity, while shortening the alkyl group by yet another carbon atom to ethyl resulted in **11** with substantially weaker hA_{2A} receptor affinity compared with **4**. Next, the effect of introducing a branch into the amide alkyl chain was explored. Replacing the *n*-butyl group with an isopropyl group (**12**), with a branching point in the α position, largely restored the affinity

Table 1. Key Parameter Data for Reference Compounds **1** and **2**, Hit Compounds **3** and **4**, and Close Analogues of **4**^a


compd	R	hA _{2A}	hA ₁	human Cl _{int} ^b (L/min)	rat Cl _{int} ^b (mL/min)	Caco-2 cell permeability		CYP P450s, IC ₅₀ (μM)				
						P _{app} (cm/s)	ratio (BA/AB) ^c	CYP1A2	CYP2C9	CYP2C19	CYP2D6	CYP3A4
1		72	3000	0.1	11	120	0.7	>40	13	>40	>40	>40
2		5	30% ^e	<i>f</i>	<i>f</i>	4.5	1.1	>40	<i>f</i>	>40	>40	<i>f</i>
3	<i>o</i> -tolyl	220	47%	0.5	5	84	0.8	>40	>40	23	>40	1.4
4	<i>n</i> -butyl	190	69%	2.3	54	77	0.7	>40	40	>40	>40	>40
10	<i>n</i> -propyl	350	54%	0.8	18	120	0.7	>40	>40	36	>40	>40
11	ethyl	890 ^d	31% ^d	<i>f</i>	<i>f</i>	<i>f</i>	<i>f</i>	<i>f</i>	<i>f</i>	<i>f</i>	<i>f</i>	<i>f</i>
12	isopropyl	300 ^d	<i>f</i>	<i>f</i>	<i>f</i>	<i>f</i>	<i>f</i>	<i>f</i>	<i>f</i>	<i>f</i>	<i>f</i>	<i>f</i>
13	isobutyl	90	64%	1.6	12	110	0.7	>40	>40	>40	>40	>40
14	neopentyl	36	39%	0.7	11	110	0.7	>40	>40	>40	>40	>40

^a Affinities at hA_{2A} and hA₁ receptors are expressed as K_i values (nM) or as percent displacement of radioligands at a compound test concentration of 10 μM, as indicated. Data are means of at least 2 determinations unless otherwise noted. ^b Intrinsic clearance measured in incubations of compounds with liver microsomes of human or rat origin, as indicated. ^c Efflux ratio expressed as the ratio between membrane permeability in the basolateral to apical (BA) versus apical to basolateral (AB) directions. ^d n = 1. ^e Test concentration = 2000 nM. ^f Not tested.

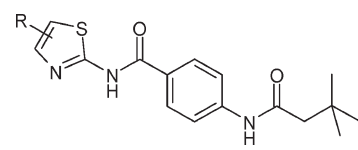


- 5:** R = H
6: R = 2-Cl
7: R = 2-OMe
8: R = 3-Me
9: R = 4-Me

Figure 1. Close analogues of hit **3**.

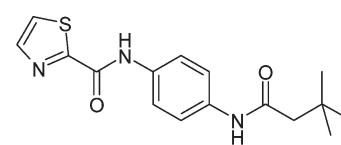
toward the hA_{2A} receptor to the level of **4**, while introducing an isobutyl group as the amide substituent, with a branching point in the β position of the alkyl chain, gave **13** with higher hA_{2A} receptor affinity compared with **4**. Adding another methyl group to the β position of the alkyl chain as in the neopentyl group, gave **14** with the highest hA_{2A} receptor affinity in this initial structure–activity relationship (SAR) investigation. Also, **14** had low human and rat microsomal clearance, an excellent Caco-2 cell membrane permeability with no indication of active efflux, and a clean CYP enzyme inhibition profile. In general, low human and rat microsomal clearance, good membrane permeability properties without active efflux, and lack of CYP enzyme inhibition appeared to pertain to the series. Also, none of the compounds showed potent affinity toward the hA₁ receptor.

Compound **14** was taken as a starting point to further investigate the series. To explore the SAR of the 2-aminothiazol amide moiety, the compounds in Table 2 and Figure 2 were prepared. Introducing a 5-chloro substituent on the thiazole ring (**15**) gave a compound equipotent to **14** at the hA_{2A} receptor, while a 5-methyl substituent (**16**) led to a modest loss in hA_{2A} receptor affinity compared with **14**. However, both **15** and **16** had lower selectivity toward the hA₁ receptor compared with **14**. In contrast, 4,5-dimethyl substitution of the thiazole ring was less well tolerated at the hA_{2A} receptor (**17**). Inversion of the 2-aminothiazol amide

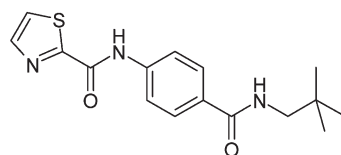
Table 2. SAR of Thiazole Substitution of **14** at hA_{2A} and hA₁ Receptors^a


compound	R	hA _{2A} K _i (nM)	hA ₁ K _i (nM)
15	5-Cl	28	220
16	5-Me	120 ^b	1100 ^b
17	4,5-di-Me	220	<i>c</i>

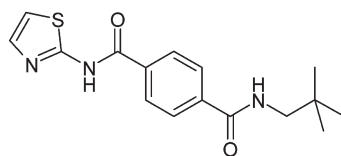
^a Data are means of at least two determinations unless otherwise noted. ^b n = 1. ^c Not tested.



18: hA_{2A}: 18% inhib.@ 10 μM

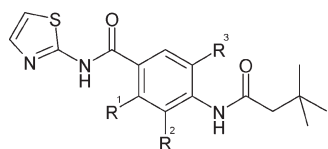


19: hA_{2A}: 0% inhib.@ 10 μM



20: hA_{2A}: K_i = 110 nM

Figure 2. Structures and hA_{2A} receptor affinities of inverted amides analogues of **14**.

Table 3. SAR of Phenyl Ring Substituted Analogues of **14**^a

compound	R ¹	R ²	R ³	hA _{2A} K _i (nM)	hA ₁ K _i (nM)	hA ₁ / hA _{2A}
14	H	H	H	36	39%	
21	OMe	H	H	50	1100	22
22	Me	H	H	200 ^b	36% ^b	
23	Cl	H	H	180	14%	
24	H	OMe	H	17	340	20
25	H	Me	H	19	460	24
26	H	Cl	H	22	210	10
27	H	F	H	9.2	650	71
28	H	F	F	5.9	410	69
29	H	Cl	Me	32	580	18
30	OMe	F	H	12	220	18

^a Affinities at hA_{2A} and hA₁ receptors are expressed as K_i values (nM) or as percent displacement of radioligand at a compound test concentration of 10 μM as indicated. Data are means of at least two determinations unless otherwise indicated. ^b n = 1.

led to a complete loss of hA_{2A} receptor affinity, irrespective of the orientation of the other amide (**18** and **19**) (Figure 2). The carboxamide could be inverted if the original orientation of the 2-aminothiazol amide was preserved, albeit with a moderate drop in hA_{2A} receptor affinity (**20**). This suggested that the 2-aminothiazol amide is strongly involved in the interaction with the hA_{2A} receptor. We next examined the effects of substitution at the phenyl ring. The results are summarized in Table 3. Generally, a substituent in the R¹ position resulted in compounds with lower affinity for the hA_{2A} receptor (**21–23**), while compounds with higher hA_{2A} receptor affinity than **14** could be obtained through substitution at the R² position, with fluorine giving the most pronounced effect (**27**). In particular, fluorine substituents in both the R² and R³ positions yielded the most potent compound **28**. In contrast, no improvement in potency was obtained from the combination of a chloro and a methyl substituent in the R² and R³ positions (**29** vs **25** and **26**). Combining a fluorine substituent in R² with a methoxy substituent as the most favorable R¹ substituent also did not lead to improved affinity (**30** vs **27**). Generally, a parallel SAR for hA_{2A} and hA₁ receptor affinity was observed. Overall, halogen and especially fluoro substitution in the R² position appeared to be optimal with respect to both hA_{2A} receptor affinity and selectivity toward hA₁ receptors. Compound **28** with fluorine substituents at both the R² and the R³ positions emerged from this series as the most potent compound with a K_i value for the hA_{2A} receptor of 5.9 nM and a selectivity ratio toward the hA₁ receptor of 69, which is in the range of **1**.

Molecular Modeling. Docking of 28 into the hA_{2A} Receptor X-ray Structure. At the time of lead optimization of the series, a crystal structure was not available for the A_{2A} receptor to support a structure-based design program. Recently, an X-ray structure of the A_{2A} receptor in complex with the antagonist ZM241385 (Figure 3 right-hand panels) became available,²⁴ and successful docking campaigns into the crystal structure to discover new ligands to the receptor

were recently reported.^{25,26} In the light of these developments, we docked **28** into the crystal structure of the A_{2A} receptor to explore the most likely binding mode and key binding site interactions.

The binding mode of the best scoring Glide²⁷ docking pose of **28** was found to be in overall agreement with the binding interactions observed for ZM241385 (Figure 3). The aromatic 2-aminothiazol amide region was in its lowest energy conformation and was well aligned to the hydrophobic clamp between Phe168 and Ile274/Leu249, in the same way as was observed for the triazolotriazine-furan part of ZM241385. The polar interactions of **28** to Asn253 were somewhat different from the observed interactions with ZM241385, due to the structural differences between these molecules. In our docking pose of **28**, the thiazole nitrogen acted as a hydrogen bond acceptor to form a strong hydrogen bond (~3 Å) with the side chain amide-NH of Asn253 as the donor; while in ZM241385, weaker hydrogen bonds to the Asn253 side-chain amide were observed from the oxygen of the furan (3.3 Å) and a triazolone nitrogen (3.6 Å). Compound **28** has no hydrogen bond donor in an equivalent position to the exocyclic amino group in ZM241385, which forms a hydrogen bond to the side chain carbonyl of Asn253. However, if a bridging water is inserted between the 2-aminothiazol amide-NH of **28** and the side chain carbonyl of Asn253, this hydrogen-bonding network may partly explain the strong affinity of **28** for the hA_{2A} receptor (see Figure 3). Evidence to support this binding mode includes that inversion of the 2-aminothiazol amide resulted in the completely inactive compounds **18** and **19** (Figure 2), indicating a highly sensitive region of the compounds with respect to polar interactions, since **18**, **19**, and **28** can adopt similar overall shapes. The neopentyl carboxamide part of **28** was also docked in a low-energy conformation with the amide slightly out of the plane of the aryl ring, due to its two fluorine ortho-substituents. The neopentyl part of **28** occupies the same area (close to the extracellular loop 2) as the phenolic “tail” of ZM241385. Although this region of the compound structures contributed significantly to the affinity of the compounds (Table 1), it was less obvious to pinpoint any specific interactions with the receptor binding pocket. The less specific nature of this part of the receptor binding pocket is also supported by the allowed inversion of the carboxamide, as exemplified by **20**. A potential explanation for the differences in affinity of the compounds as a function of substituents in this region is displacement of high-energy waters from the receptor site as recently described for this region of the A_{2A} receptor.²⁸

In Vitro Characterization of 28 for hA_{2A} Receptor Antagonism and Selectivity. The efficacy of **28** as an antagonist at the hA_{2A} receptor was demonstrated in a functional cAMP assay using AlphaScreen technology (PerkinElmer) with CHO cells expressing the human A_{2A} receptors. The cells were stimulated with the adenosine receptor agonist N-ethylcarboxamidoadenosine (NECA), and concentration–response curves were generated in the presence of **28** at five fixed concentrations. Compound **28** caused right shifting of the concentration–response curves of NECA, and a Schild analysis revealed that **28** is a competitive antagonist with a K_b of 1.3 nM, which is in good agreement with the K_i value of 5.9 nM (Figure 4).

The selectivity of **28** with respect to binding to the hA_{2B} and hA₃ subtypes of the adenosine receptor family was investigated by displacement of [³H]MRS1754 from hA_{2B} receptors expressed in a human embryonic kidney (HEK-293)

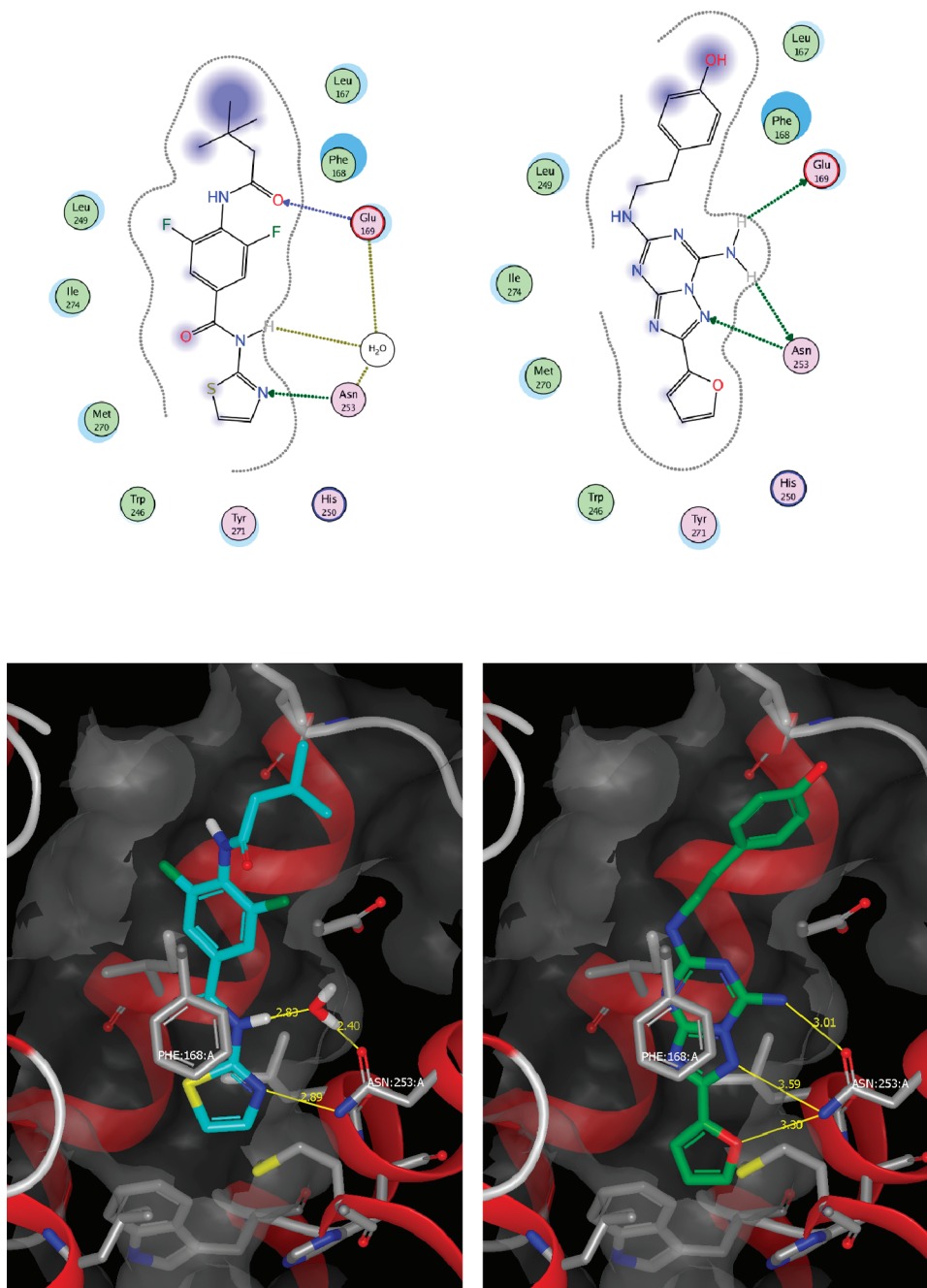


Figure 3. (Top) Schematic representation of the A_{2A} receptor binding site interactions with **28** (left panel) and ZM241385 (right panel) created with the “Ligand Interactions” tool in MOE. The dashed lines indicate a proximity contour, and residues are colored according to their lipophilic or polar properties; a blue shade behind a residue indicates receptor–ligand contact. Donor/acceptor and water contacts are outlined with dashed arrows (green for side chain and blue for backbone contacts). (Bottom) The A_{2A} receptor binding site interactions with **28** (left panel) and ZM241385 (right panel) viewed from TM5, which is partly removed for clarity. The docking pose of **28** (cyan) with interstitial water mediating an interaction between **28** and Asn253 is modeled, compared with the X-ray structure of ZM241385 (green). The yellow lines indicate hydrogen bond interactions (length). Contact residues within 4 Å of the ligand are shown in stick mode (others are hidden).

cell line, and displacement of [³H]-AB-MECA from hA₃ receptors expressed in a CHO-K1 cell line. At hA_{2B} receptors, **28** had a K_i of 260 nM, and at hA₃ receptors, **28** gave 36% inhibition of binding at a test concentration of 10 μM, suggesting a $K_i > 10\,000$ nM. Thus, the selectivity ratio of **28** toward the other members of the adenosine receptor family was 69-fold versus the hA₁ receptor, 45-fold versus the hA_{2B} receptor, and >1000-fold versus the hA₃ receptor.

Compound **28** was also tested in a broad pharmacology panel screen against 60 receptors, ion channels, and transporters. At all targets, **28** displayed less than 30% inhibition

of binding at a 10 μM test concentration, suggesting a highly selective pharmacological profile of the compound (for details, see Supporting Information).

ADME Profile of 28. To evaluate the drug-like properties of **28**, a detailed *in vitro* and *in vivo* ADME characterization was performed, and key data are summarized in Tables 4 and 5.

Compound **28** was characterized by high membrane permeability (Caco-2 $P_{app,A-B} = 88 \times 10^{-6}$ cm/s), which translates into rapid absorption *in vivo* from the gastrointestinal tract and distribution between brain and plasma. No significant

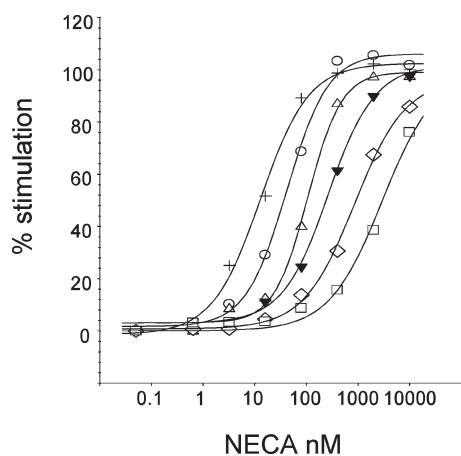


Figure 4. Antagonist effect of **28** at hA_{2A} receptors against the agonist NECA (A_{2A} agonist) measured as stimulation of cAMP formation using AlphaScreen technology. EC_{50} determinations of NECA were performed in the absence (+) or in the presence of five concentrations of **28** (2.5 nM (○), 7.4 nM (△), 22 nM (▼), 66.7 nM (◇) and 200 nM (□)) in CHO cells expressing human A_{2A} receptors. The plot represents a single experiment. The K_i was determined as 1.3 nM by Schild analysis (means of three values).

Table 4. *In Vitro* ADME Parameters for **28**^a

assay	conc (μM)	rat	dog	human
hepatocyte CL_{int} (mL/min) ^b	0.2	12	346	600
Caco-2 $P_{app,A-B}$ (cm/s × 10 ⁶)	1.0			88 ± 7
$P_{app,B-A}$ (cm/s × 10 ⁶)	1.0			67 ± 7
serum protein binding (%) ^b	1.0	97	87	85

^aMean ± SD ($n = 3$). ^b $n = 1$.

Table 5. *In vivo* PK Parameters and Standard Deviation for **28** in Sprague–Dawley Rats Following Administration of 0.5 mg/kg iv ($n = 3$) and 1 mg/kg po ($n = 3$)

PK parameter	value	SD
T_{max} (h) ^a	0.5	0.1
C_{max} (ng/mL) ^a	878	406
F (%) ^a	88	25
CL_p (L/h/kg)	0.3	0.1
V_{ss} (L/kg)	1.0	0.3
$t_{1/2,\alpha}$ (h)	1.2	0.3
f_α	0.9	0.1
$t_{1/2,\beta}$ (h)	7.8	2.1
f_β	0.1	0.0

^aValues based on po data.

involvement of active transport was indicated in the Caco-2 assay or *in vivo* using P-gp (abcb1a)-deficient mutant mice. The whole-brain/plasma ratio was 0.8 ± 0.3 in mice (1 mg/kg po, 50 min).

No significant inhibition of CYP 1A2, 2D6, 2C9, 2C19, and 3A4 enzymes was found for **28** ($IC_{50} > 40 \mu M$). Serum protein binding of **28** was in the range from 85% to 97% determined *in vitro* in spiked samples of rat, dog, and human origin.

The *in vivo* PK was determined in rats following intravenous and oral administration of **28**. A low systemic clearance (0.3 L/h/kg) was observed in accordance with the low intrinsic clearance in rat hepatocytes (12 mL/min) and high degree of protein binding *in vitro*. Furthermore, a high oral bioavailability ($F = 88\%$) was found for a solubilized formulation (1 mg/kg in 25%

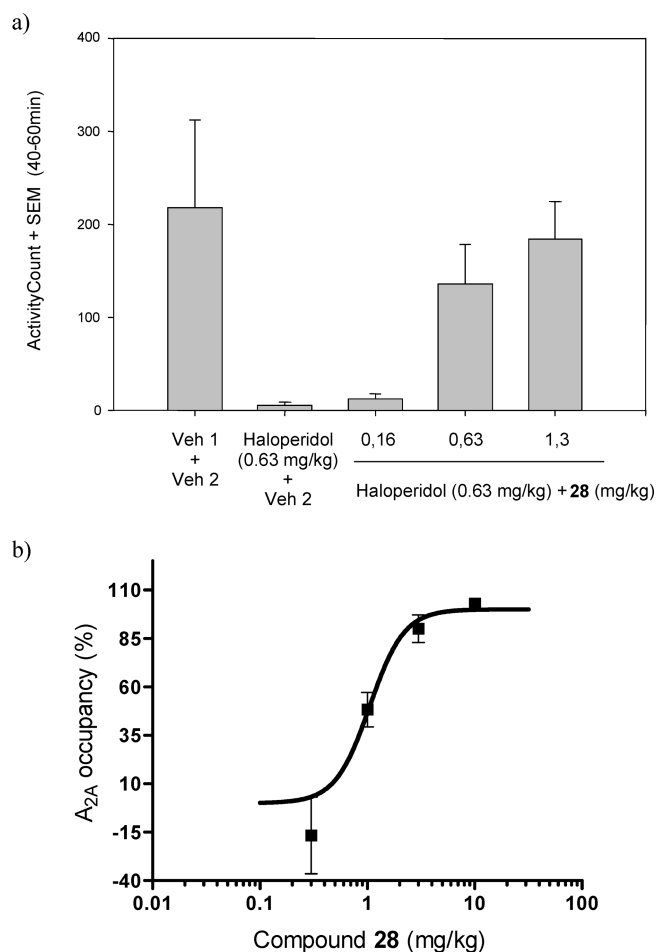


Figure 5. *In vivo* effect of **28**: (a) dose–response of **28** in haloperidol-induced hypolocomotion in mice; the ED_{50} value was determined to be 0.5 mg/kg ($n = 8$ for all groups; vehicle 1 = 0.03% PEG/0.0003% tartaric acid in deionized water; vehicle 2 = 25% cremophore/isotonic saline); (b) dose–response of displacement of [³H]-SCH58261 by **28** *in vivo* in mice. The ED_{50} was determined to be 1.1 mg/kg.

cremophore) consistent with a low hepatic extraction ratio. To assess the primary human PK properties of **28**, predictions of clearance, volume of distribution, and effective plasma half-life were performed. By combination of the results from intrinsic clearance, unbound fractions in serum, and the *in vivo* clearance in rats, the *in vitro/in vivo* extrapolated intravenous human hepatic clearance for **28** was predicted to be around 29 L/h (for a 70 kg subject), and hence **28** has a low hepatic extraction ratio relative to the human liver blood flow, which is around 90 L/h.^{29,30} When the rat volume of distribution at steady-state (V_{ss}) was extrapolated to a 70 kg human, a moderate distribution of 320 L was predicted.³¹ The corresponding predicted effective plasma half-life was around 8 h. This suggests that **28** displays acceptable PK properties for human dosing once or twice daily, depending on the PK/PD association.

In Vivo Characterization of Compound 28. Compound **28** was tested in haloperidol-induced hypolocomotion in mice.³² After po administration, **28** dose dependently and fully reversed the hypolocomotive state, with an ED_{50} value of 0.5 mg/kg (Figure 5a). For comparison, **1** and **2** reversed the induced hypolocomotive state with ED_{50} values of 0.13 mg/kg and 0.4 mg/kg, respectively. To verify that the observed behavior after dosing of **28** was correlated to blockade of A_{2A} receptors, an *in vivo* binding experiment was performed

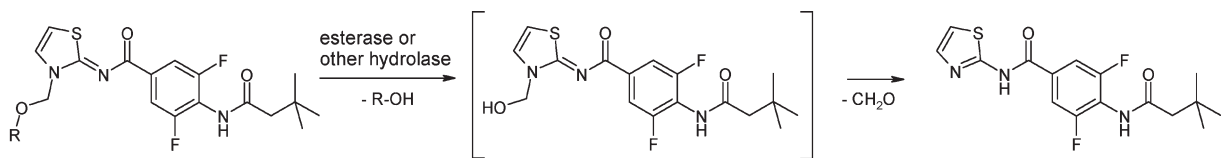
(Figure 5b). Administration of **28** dose-dependently displaced [^3H]SCH58261 with an ED_{50} of 1.1 mg/kg. This value corresponds well to the ED_{50} observed in haloperidol-induced hypolocomotion, suggesting blockade of $\text{A}_{2\text{A}}$ receptors to be the mechanism of action of the reversal of haloperidol-induced hypolocomotion.

Formulation of **28 as a Prodrug.** The *in vitro* and preliminary *in vivo* data for **28** suggested a compound of great interest. However, the otherwise excellent pharmacological profile of the compound was limited by an extremely low intrinsic solubility. This became apparent after evaluating the potential impact of the low aqueous solubility of **28** on oral bioavailability in a PK study, comparing the oral bioavailability of **28** dosed as a 5 mg/kg suspension in a methylcellulose vehicle (mean particle size 8 μm) to that of a solubilized formulation (1 mg/kg in 25% cremophore). The mean oral bioavailability of **28** was significantly reduced by formulation as a suspension (10% \pm 2%) relative to that of a solution (88% \pm 25%). This suggested that a significant penalty on oral bioavailability could arise from solid dose formulations. Various unsuccessful attempts at finding suitable formulations of **28** led us to consider the option of derivatizing the compound as a prodrug. Derivatization of drugs with low solubility as water-soluble prodrugs has recently been reviewed.^{33–36} Also, a prodrug approach has been applied to enhance the aqueous solubility of xanthine-type $\text{A}_{2\text{A}}$ receptor antagonists.³⁷ As a compound with excellent membrane permeability, **28** lent itself to a prodrug approach aimed at improving the aqueous solubility. We envisioned that by this strategy, **28** would be readily absorbed into the capillary blood vessels lining the gut, ideally without any of the prodrug entering the systemic circulation. Importantly, the pro-moiety of a prodrug should be nontoxic, and we chose to investigate the use of a phosphonoxymethyl ester and esters of the biogenic amino acids as solubility enhancing pro-moieties. Since **28** has no structural feature such as an alcohol functionality, which would allow direct attachment of a pro-moiety, transient introduction of such a group was necessary. We speculated that derivatization of the 2-aminothiazole moiety should allow for this transformation. Previous examples in the literature suggested that alkylation with chloromethylene esters of amino acids or of chloromethylphosphate esters would be an efficient way of introducing a solubilizing group via a collapsible linker.^{38–40} By this strategy, we prepared the prodrugs **31** and **32** (Lu AA47070), as outlined in Scheme 3 (*vide infra*).

Table 6. Aqueous Solubility of **28** and Prodrugs **31** and **32**

compound	aqueous solubility, $\mu\text{g/mL}$ (pH)
28	1 (7.4)
31	19400 (4.0)
32	8600 (6.9)

Scheme 1. Proposed Mechanism for the Release of **28** from **31** or **32**



31: R = (2*S*,3*S*) $\text{H}_2\text{N-CH}(\text{C}(\text{CH}_3)\text{CH}_2\text{CH}_3)\text{-CO}$

32: R = $(\text{HO})_2\text{-P}(\text{O})$

28

From the pool of biogenic amino acids, we selected isoleucine as the pro-moiety, since its two chiral centers would allow for a simple assessment of whether significant racemization would take place at the α -carbon under the reaction conditions needed to prepare **31**. No racemization was observed as investigated by NMR or HPLC/UV/MS. The regiochemistry of **31** and **32** with respect to the attachment of the pro-moieties to **28** was established via HMBC $^1\text{H-}^{13}\text{C}$ correlation NMR spectra. In both cases, a maximal three-bond distance between the linker methylene-H to thiazole C-4 was established, which excluded the possibility of the pro-moiety being attached to the amide nitrogen.

The aqueous solubility data of **28** and the prodrugs **31** and **32** are summarized in Table 6. In both cases, the prodrugs were vastly more soluble than **28**, increasing the aqueous solubility by several thousand fold. For **31**, it was necessary to keep the pH of the solutions low (< 4), since rapid chemical hydrolysis took place at physiological pH at 48 $^\circ\text{C}$ ($t_{1/2}$ = 0.4 h at pH 7). For comparison, the $t_{1/2}$ of chemical hydrolysis of **32** at pH 7 and 48 $^\circ\text{C}$ was > 1600 h (see the Supporting Information for details).

Prodrug Bioactivation. The mechanism of liberation of **28** from the prodrugs was not investigated but likely follows the sequence of steps shown in Scheme 1. The intermediary hydroxymethylene derivative of **28** was never observed, suggesting rapid breakdown and hence the hydrolysis of the pro-moiety as the rate limiting step.

To investigate the bioconversion of the prodrugs **31** and **32** into **28**, a rat PK study was performed. The prodrug **32** was

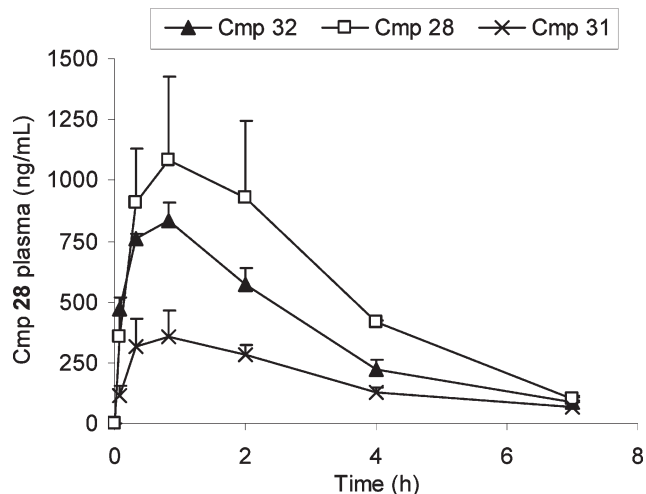
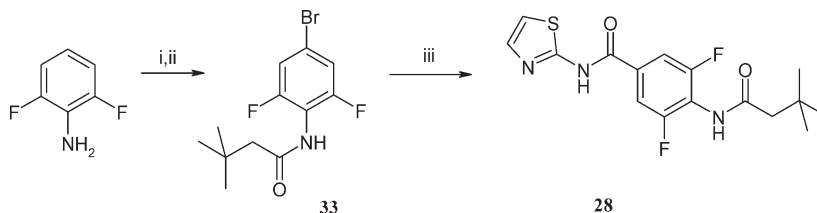
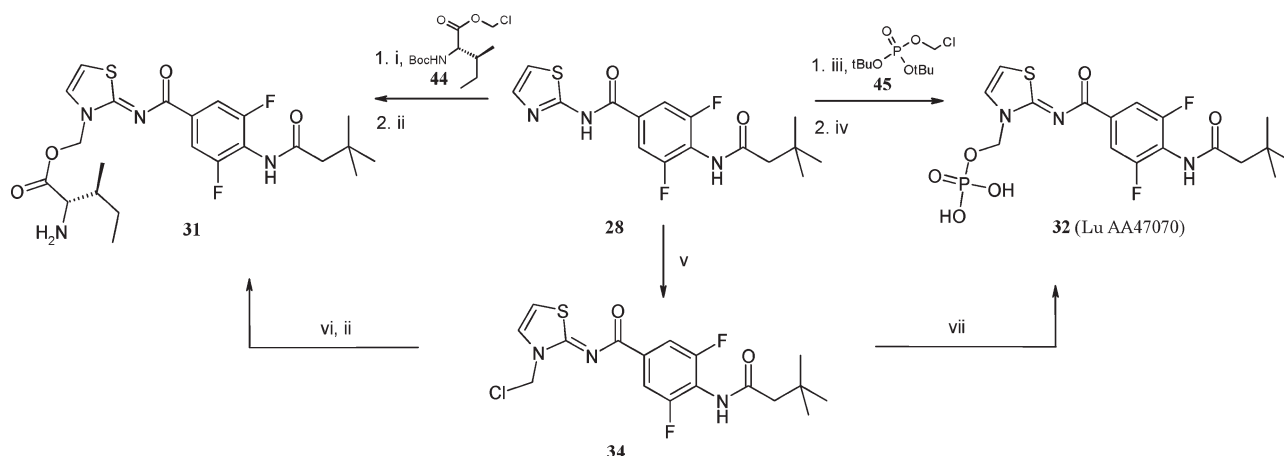


Figure 6. Plasma concentration–time profile of **28** in rats following po administration of the prodrugs **32** (1.5 mg/kg cmp **28** equivalence, $n = 3$) or **31** (1.4 mg/kg cmp **28** equivalence, $n = 3$). For comparison, the “intrinsic” PK profile for **28** (1 mg/kg po) dosed in 25% cremophore solution is also plotted ($n = 3$).

Table 7. Mean (\pm SD) Calculated PK Parameters of **28** Following po Administration of **32** (1.5 and 15 mg/kg) or **31** (1.4 mg/kg) to Rats ($n = 3$)

compound	dose ^a (mg/kg)	AUC (ng \times h/L)	T_{\max} (h)	C_{\max} (ng/mL)	F (%)
32	1.5	2.9 \pm 0.7	0.5 \pm 0.1	869 \pm 68	55 \pm 13
32	15	35 \pm 3.0	0.4 \pm 0.2	6413 \pm 281	66 \pm 6
31	1.4	1.5 \pm 0.4	0.9 \pm 0.2	381 \pm 193	31 \pm 7

^aDose equivalents of **28**.**Scheme 2.** Synthetic Method Applicable for Kilogram Scale Preparation of **28**^a^aReagents and conditions: (i) NBS, DMF, 82%; (ii) Me₃CCH₂COCl, pyridine, 1,2-DCE, 94%; (iii) 2-aminothiazole, CO (1 atm), Bu₃N, DMAc, Pd(dppf)Cl₂, 120 °C, 72%.**Scheme 3.** Preparation of Prodrugs **31** and **32** of Compound **28**^a^aReagents and conditions: (i) NaH, Boc-Ile-OCH₂Cl (**44**), DMF, 50 °C, 82%; (ii) 2 M HCl/diethylether, 100%; (iii) NaH, (*t*-BuO)₂PO-OCH₂Cl (**45**), DMF, 27%; (iv) TFA, DCM, 100%; (v) NaH, ClCH₂OCOC(=O)Cl, DMF, 96%; (vi) Boc-Ile-OH, DIPEA, DMF, 60 °C, 61%; (vii) phosphoric acid, DIPEA, MeCN, H₂O, reflux, 40%.

administered po in a dose equivalent to 1.5 mg/kg of **28**, and **31** was administered po in a dose equivalent to 1.4 mg/kg of **28**, respectively. A rapid uptake into the systemic circulation and conversion into **28** was observed for both prodrugs (Figure 6). The prodrug plasma levels were <0.5% relative to **28** during the entire sampling period. The extensive conversion of **32** resulted in a po bioavailability of **28** that was not statistically significantly different from that observed for **28** when dosed in a cremophore solution (Table 7, $P < 0.05$, Student's t test). The high intrinsic solubility of **32** was suggested to overcome the potential limitations in bioavailability (dissolution limiting) at higher doses of **28**. This was confirmed by the unchanged po bioavailability at 15 mg/kg **32**, which gave an almost dose-linear increase in plasma concentrations of **28**, reaching a C_{\max} of 6413 ng/mL.

A robust po bioavailability of **28** was also observed following po administration of the prodrug **31** ($F = 31\%$, Table 7) although the absolute bioavailability was approximately 3-fold lower than that observed for **28** dosed in solution.

Chemistry. In general, the compounds were prepared by well-established methodology. (for details, see the Supporting Information). For the larger scale preparation of compound **28**, an alternative synthesis suitable for kilogram scale

production was developed, as shown in Scheme 2. Thus, 2,6-difluoroaniline was brominated by reaction with *N*-bromosuccinimide (NBS) in DMF, followed by acylation with 3,3-dimethylbutyryl chloride in the presence of pyridine to give **33** in 82% overall yield. Compound **33** was next transformed into **28** in a Pd-catalyzed reaction with 2-aminothiazole and carbon monoxide in 72% yield.

Prodrugs of **28** were synthesized as detailed in Scheme 3. First, **28** was deprotonated with sodium hydride, and reaction with Boc-isoleucine-chloromethylene ester **44**³⁸ followed by acid-mediated deprotection provided **31** in 82% overall yield. Similarly, deprotonation of **28** with sodium hydride followed by reaction with di-tert-butyl-chloro-methylene phosphate ester **45**³⁹ and deprotection with trifluoroacetic acid (TFA) in dichloromethane (DCM), yielded the phosphonoxymethylene prodrug **32** in 27% overall yield.

While attempts to prepare and isolate the hydroxymethylene adduct of **28** as a common prodrug precursor were unsuccessful, we serendipitously discovered that the chloromethylene derivative **34** was easily obtained. Thus, deprotonation of **28** with sodium hydride and subsequent reaction with chloromethyl chloroformate yielded intermediate **34** in 96% yield. Reaction of the stable intermediate **34** with the corresponding

acids, Boc-isoleucine and phosphoric acid, was the preferred method to prepare **31** (61% yield) and **32** (40% yield), respectively (Scheme 3).

Conclusion

Herein we have disclosed the discovery and SAR of a novel structural class of hA_{2A} receptor antagonists. Lead optimization starting from two moderately potent screening hits **3** and **4** resulted in the identification of a potent and selective hA_{2A} receptor antagonist (**28**). Compound **28** was shown to be selective for the hA_{2A} receptor among the adenosine receptor subtypes as well as in a broad pharmacology panel screen of 60 GPCRs, ion channels, and transporters. *In vitro* and *in vivo* ADME characterization suggested drug-like properties of **28**, and the compound was active in haloperidol-induced hypolocomotion in mice, an *in vivo* model of Parkinson's disease (ED₅₀ = 0.5 mg/kg). Also, **28** displaced the A_{2A} receptor selective radioligand [³H]-SCH58261 in an *in vivo* binding experiment (ED₅₀ = 1.1 mg/kg), suggesting the reversal of haloperidol-induced hypolocomotion to be mediated by A_{2A} receptor blockade. However, the aqueous solubility of **28** limited its potential as a drug candidate. The improved ADME profile of **28** achieved via the water-soluble prodrug **32** allowed for a more detailed preclinical evaluation, which will be reported in a future publication.

Experimental Section

General Chemistry. ¹H NMR spectra (500 MHz) were recorded on a Bruker Avance AV-III-500 spectrometer. ¹H NMR spectra (600 MHz) were recorded on a Bruker Avance AV-III-600 spectrometer. Chemical shift values are expressed in ppm relative to Me₄Si. Preparative HPLC purification with MS detection was performed on a Sciex API150ex preparative LC/MS system equipped with a Gilson 333 pump (master) and a Gilson 334 pump (slave) and an Applied Biosystems API150ex single quadrupole mass spectrometer with atmospheric pressure photoionization (APPI) ion source. The purities of the intermediates and final compounds were determined by integration of the UV signal obtained by analytical HPLC–UV–MS on a Sciex API150ex analytical LC/MS system equipped with three Shimadzu LC10ADvp LC pumps, a Shimadzu SPD-M20A photodiode array UV detector, and an Applied Biosystems API150ex single quadrupole mass spectrometer with an atmospheric pressure photoionization (APPI) ion source or by integration of the UV-signal obtained by analytical HPLC–UV–MS on a Sciex API300 analytical LC/MS system equipped with three Shimadzu LC10ADvp LC pumps, an Acquity UPLC PDA detector with an analytical flow cell, and an Applied Biosystems API300 triple quadrupole mass spectrometer with an atmospheric pressure photoionization (APPI) ion source.

Chromatography was performed on silica gel 60 (230–400 mesh ASTM), Merck.

Compounds **1**⁴¹ and **2**²³ were prepared according to the cited literature procedures. Reagents **44** and **45** were prepared as described in refs 38 and 39, respectively. Compounds **3** and **4** were obtained from commercial sources.

The purity of compounds, measured as described above, was > 95% unless otherwise stated.

Procedure Applicable for Kilogram-Scale Preparation of 28. *N*-(4-Bromo-2,6-difluoro-phenyl)-3,3-dimethyl-butylamide (**33**). 2,6-Difluoroaniline (1.5 mL, 14 mmol) was dissolved in 15 mL of DMF, and NBS (2.5 g, 14 mmol) added portion-wise. After the last addition the reaction was stirred for ca. 30 min and then poured into water. The formed precipitate was collected by filtration, washed with water, and dried *in vacuo*. The brominated product was dissolved in 20 mL of 1,2-DCE, and pyridine (1.1 mL, 14 mmol) was added and then 3,3-dimethyl-butyl chloride (1.95 mL,

14 mmol) was added dropwise, and the reaction was stirred at room temperature for 18 h. The reaction mixture was poured into 2 M HCl and extracted with ethyl acetate, and the organic extracts were dried on MgSO₄, filtered, and evaporated. The obtained solid was recrystallized from EtOH/H₂O. The product was used without further purification. Yield: 2.18 g (75%). ¹H NMR (*d*₆-DMSO): 1.03 (s, 9H); 2.21 (s, 2H); 7.50–7.55 (2H); 9.58 (br s, 1H).

4-(3,3-Dimethyl-butylamino)-3,5-difluoro-*N*-thiazol-2-yl-benzamide (28). Compound **33** (34.1 g, 164 mmol), 2-aminothiazole (16.7 g, 167 mmol), Pd(dppf)Cl₂ (0.65 g, 0.8 mmol), and Bu₃N (50 mL, 212 mmol) was suspended in 70 mL of dimethylacetamide (DMAc) in an autoclave. The container was degassed and filled with CO(g) three times, then the reaction mixture was heated to 120 °C and stirred vigorously for 18 h. The reaction mixture was cooled and filtered through a pad of Celite and was then diluted with acetonitrile. The precipitated product was collected, washed with acetonitrile, and crystallized from MeOH. Melting point: 258 °C. Yield: 41.7 g (72%). ¹H NMR (*d*₆-DMSO): 1.05 (s, 9H); 2.27 (s, 2H); 7.32 (d, 1H); 7.59 (d, 1H); 7.90 (d, 2H); 9.83 (s, 1H); 12.82 (br, 1H).

Preparation of Prodrugs. (2*S*,3*S*)-2-Amino-3-methyl-pentanoic Acid 2-[(*E*/*Z*)-4-(3,3-Dimethyl-butylamino)-3,5-difluoro-benzoylimino]-thiazol-3-ylmethyl Ester, Hydrochloride Salt (31). NaH (60% in mineral oil suspension; 0.19 g, 4.8 mmol) was suspended in 10 mL of DMF, and compound **28** (1.4 g, 4 mmol) was added. The mixture was stirred for 1 h or until it became a clear solution. At this point, **44** (1.1 g, 4 mmol) was added, and the reaction mixture was stirred at 50 °C overnight. The solvent was evaporated, and the crude was purified by flash chromatography on silica using 10% ethyl acetate in DCM as eluent. The obtained product was treated with 2 M HCl/diethyl ether for 1 h, and the solvent was evaporated. The product was dried *in vacuo* overnight to yield **31** as an amorphous solid. Yield: 1.74 g (82%). ¹H NMR (*d*₆-DMSO): 0.70 (t, 3H); 0.79 (d, 3H); 1.05 (s, 9H); 1.17 (m, 1H); 1.33 (m, 1H); 1.84 (m, 1H); 2.26 (s, 2H); 4.08 (m, 1H); 6.32 (d, 1H); 6.51 (d, 1H); 7.15 (d, 1H); 7.74 (d, 1H); 7.86 (d, 2H); 8.48 (br, 2H); 9.76 (s, 1H).

Phosphoric Acid Mono-2-[(*E*/*Z*)-4-(3,3-dimethyl-butylamino)-3,5-difluoro-benzoylimino]-thiazol-3-ylmethyl Ester (32). Compound **32** was prepared as described for **31**, using compound **45**. Deprotection was effected by dissolving the obtained product in DCM containing 5 equiv of TFA. The deprotection mixture was stirred at room temperature for 16 h. A formed precipitate, which was the desired product, was collected by filtration, washed with DCM, and dried *in vacuo*. Crystallization from THF/ethyl acetate (1:1) gave a crystalline material, which melted with decomposition at 216–220 °C. Yield: 0.11 g (27%). ¹H NMR (*d*₆-DMSO): 1.05 (s, 9H); 2.25 (s, 2H); 6.02 (s, 1H); 6.04 (s, 1H); 7.12 (d, 1H); 7.65 (d, 1H); 7.92 (d, 2H); 9.72 (s, 1H).

Alternative Preparation of Prodrugs from Common Intermediate 34. *N*-[3-Chloromethyl-3*H*-thiazol-(2-*E*/*Z*)-ylidene]-4-(3,3-dimethyl-butylamino)-3,5-difluoro-benzamide (**34**). NaH (60% in mineral oil suspension; 0.8 g, 20 mmol) was suspended in 100 mL of DMF, and compound **28** (6 g, 17 mmol) was added. The mixture was stirred at room temperature for 1 h or until the solids had dissolved. The reaction mixture was then cooled to 0 °C, and chloromethylchloroformate (4.3 mL, 50 mmol) was added dropwise. Stirring was continued at room temperature overnight. To the reaction mixture were added ethyl acetate and water, and the phases were separated. The organic phase was washed twice with sat. NH₄Cl (aq) and then with water, then it was dried on MgSO₄, filtered, and evaporated to give the product as a white solid. Yield: 6.5 g (96%). ¹H NMR (*d*₆-DMSO): 1.05 (s, 9H); 2.25 (s, 2H); 6.31 (s, 2H); 7.19 (d, 1H); 7.75 (d, 1H); 7.92 (d, 2H); 9.75 (s, 1H).

(2*S*,3*S*)-2-Amino-3-methyl-pentanoic Acid 2-[(*E*/*Z*)-4-(3,3-Dimethyl-butylamino)-3,5-difluoro-benzoylimino]-thiazol-3-ylmethyl Ester, Hydrochloride Salt (31). Compound **34** (0.2 g, 0.5 mmol), Boc-isoleucine (0.115 g, 0.5 mmol), and DIPEA (124 μL, 0.75 mmol) were dissolved in 3 mL of DMF, and the solution was stirred at 60 °C for 2 h. The reaction mixture was diluted with water and extracted three times with ethyl

acetate. The combined organic extracts were washed with brine, dried on MgSO_4 , filtered, and evaporated. The crude product was purified by chromatography on silica using 30% ethyl acetate in heptane as eluent. Deprotection was effected by treatment with 2 M HCl/diethyl ether for 1 h; then the solvent was evaporated, and the product was dried *in vacuo* overnight to yield the product as an amorphous solid. The residue was pure product with identical data as described above. Yield: 0.16 g (61%).

Phosphoric Acid Mono-[(*E/Z*)-4-(3,3-dimethyl-butylamino)-3,5-difluoro-benzoylimino]-thiazol-3-ylmethyl} Ester (32). Compound **34** (24.8 g, 62 mmol) was dissolved in 150 mL of acetonitrile, and 85% phosphoric acid (23 mL, 400 mmol) and DIPEA (8.3 mL, 500 mmol) were added. The reaction mixture was refluxed for 2 h and then cooled to room temperature. Water (200 mL) and THF (100 mL) were added together with 30 mL of conc. $\text{NH}_3(\text{aq})$, and the phases were separated. The organic phase was washed with 50 mL of water and 15 mL of conc. $\text{NH}_3(\text{aq})$, and the combined aqueous phases were added to 200 mL of THF and were acidified with ca. 60 mL of conc. HCl. The phases were separated, and the aqueous phase was extracted with 50 mL of THF, and then the combined organic phases were washed with water and evaporated to dryness. The residue was crystallized from THF/ethyl acetate (1:1) to yield the pure and crystalline product with identical data as described above. Yield: 11.5 g (40%).

Receptor Docking. The docking experiment was performed using Glide XP⁴² as implemented in Maestro 9.0.²⁷ The preparation of the $\text{A}_{2\text{A}}$ receptor structure (PDB code 3EML) was done with the Protein Preparation Wizard in Maestro using the default settings. All waters were removed from the prepared structure before the final generation of the docking grid. The docking poses were evaluated using the E-model scoring function in Glide. The subsequent refinement and modeling of the interstitial water was done with MOE⁴³ on the structure prepared for docking. In MOE, the refinement was done using the MMFF force field with fixed potentials for receptor atoms with exceptions of side-chain atoms within 4.5 Å of the ligand. The graphical representations of the binding site are created with the help of the "Ligand Interactions" tool in MOE.⁴⁴

Determination of Aqueous Solubility. To determine solubility of compounds, approximately 5 mg of sample was weighed into 4 mL glass vials. Assay medium (1 mL of 25 mM phosphate buffer, pH 7.4, for **28** and **32** or water for **31**) was added, and the sample was sonicated for 3 min and then shaken overnight. If the compound had completely dissolved, another 5–10 mg sample was weighed in, sonicated, and shaken overnight. The sample was then filtered through a 0.22 μm PVDF filter and analyzed by HPLC to determine the concentration of sample in solution. The concentration in solution was calculated based on a standard curve generated from known dilutions of authentic sample.

Chemical Hydrolysis Stability Assay. To determine the hydrolysis stability of a prodrug, approximately 4 mg of the sample was weighed into 4 mL glass vials. Two milliliters of water was added, and the sample was sonicated for 5 min. The sample was then filtered through a 0.22 μm PVDF filter to eliminate undissolved impurities. This stock solution was diluted into buffers of different pH to a concentration of approximately 0.05 mg/mL. Each buffer solution was split into 10 sealed glass vials. One sample from each buffer solution of compound was immediately analyzed by HPLC to determine the concentration of sample in solution based on a standard curve generated from known dilutions of authentic sample. The stability assay was accelerated by storing the sealed glass vials at 50 °C. The storage time was continuously evaluated depending on the rate of the reaction. The stored samples were diluted 1:1 with acetonitrile to ensure dissolution of possible precipitated hydrolysis products prior to analysis by HPLC, and concentration of both the prodrug and the hydrolysis products was evaluated.

Biological Methods. Membrane Preparations for $\text{hA}_{2\text{A}}$ Receptor Binding Analysis. The human $\text{A}_{2\text{A}}$ encoding DNA were

excised from the pCIneo constructs by *MluI* and *XbaI* and subcloned into the pFASTBAC2 vector cut with *XbaI* and *BssHII*. The inserts were recombined into the baculo vector using the Bac-to-Bac system (Invitrogen). The generation and isolation of baculo virus was performed as described by the distributor (Invitrogen). High Five cells (Invitrogen) were grown at 27 °C in suspension to a density of 1×10^6 and infected with a multiplicity of infection of 0.5. The cells were harvested 72 h post-infection, and membranes were prepared. Membrane aliquots were stored at -80 °C. On the day of experiment an aliquot of membranes was homogenized in 50 mM Tris/HCl buffer, pH 7.4, using an Ultra-Turrax homogenizer. The membranes were diluted to a concentration of 0.6 mg/mL and 2 U of adenosine deaminase per milliliter of membrane suspension was added (Roche Molecular Biochemicals, Nutley, NJ). The solution was preincubated 30 min at 37 °C before use.

$\text{hA}_{2\text{A}}$ Receptor Binding Analysis. Binding assay was performed in 96 well plates in a total volume of 200 μL in 50 mM Tris/HCl buffer (pH 7.4). Membranes (10.6 μg of protein/well) were incubated with compounds (10 concentrations of compounds) and 1 nM final concentration of [³H]-ZM241385 (R1036 from Tocris Cookson, Ltd., UK) for 30 min at 25 °C. After the incubation, bound ligand was separated from unbound by filtration over Unifilter GF/B presoaked in 0.1% PEI for 30 min. Filters were washed 3 times with 1 mL of ice-cold buffer and dried at 50 °C, and 35 μL of scintillation liquid was added to the filters. Bound radioactivity was counted in MicroBeta from Perkin-Elmer. Non-specific binding was determined in the presence of CGS15943.

Membrane Preparations for hA_1 Receptor Binding Analysis. CHO cells expressing A_1 receptors were grown in 58 cm^2 dishes for 3–4 days at 37 °C in 5% CO_2 and harvested when the cells were about 90% confluent. The cells were washed twice with PBS buffer, and cells were detached by scraping in buffer. The cells were centrifuged for 7 min at 1000g, and the pellet was homogenized with Ultra-Turrax in 50 mM Tris, pH 7.4, and resuspended in 2 mL/plate. Membrane aliquots were stored at -80 °C. On the day of experiment, the membranes were diluted to a concentration of 0.6 mg/mL, and 2 U of adenosine deaminase per milliliter of membrane suspension was added (Roche Molecular Biochemicals, Nutley, NJ). The solution was preincubated 30 min at 37 °C before use.

hA_1 Receptor Binding Analysis. Binding assay was performed in 96 well plates in a total volume of 200 μL in 50 mM Tris/HCl buffer (pH 7.4). Membranes (10.8 μg of protein/well) were incubated with compounds (10 concentrations of compounds) and 1 nM final concentration of [³H]-DPCPX (Amersham Biosciences, NL) for 30 min at 25 °C. After the incubation, bound ligand was separated from unbound by filtration over Unifilter GF/B presoaked in 0.1% PEI for 30 min. Filters were washed 3 times with 1 mL of ice-cold buffer and dried at 50 °C, and 35 μL of scintillation liquid was added to the filters. Bound radioactivity was counted in MicroBeta from Perkin-Elmer. Non-specific binding was determined in the presence of CGS15943.

Functional $\text{hA}_{2\text{A}}$ (cAMP) Assay. CHO cells transfected with $\text{hA}_{2\text{A}}$ receptor were used. All cells were cultured in F12 K nutrient mixture supplemented with 10% BCS, 1% glutamine, 1% penicillin, and 1% streptomycin at 37 °C in 5% CO_2 .

Twenty-four hours prior to assays, the cells were seeded into 96-half area well TC-plates from Co-star (cat. no. 3875) at 10000 cells/well in 100 μL . The next day, the cells were washed 3 times with PBS. To each well, 10 μL of acceptor beads (2 units/well) and 10 μL of test compounds were added in assay buffer of Hank's balanced salt solution (138 mM NaCl, 5 mM KCl, 1.3 mM CaCl_2 , 0.5 mM MgCl_2 , 0.4 mM MgSO_4 , 0.3 mM KH_2PO_4 , 0.3 mM Na_2HPO_4 , 5.6 mM glucose) plus 5 mM HEPES, pH 7.4, and 0.1% BSA. Plates were incubated on a shaker for 30 min in the dark at room temperature. The reaction was stopped by adding 30 μL of lysis buffer (5 mM HEPES with 0.3% Tween 20 and 0.1% BSA) containing 2 units of donor beads and 6.6 units of biotinylated cAMP. The acceptor and donor beads were from an

AlphaScreen kit from Perkin-Elmer (cat. no. 6760600R). Plates were incubated 60 min in the dark with soft shaking and finally read on a Fusion from Perkin-Elmer in Alpha Fusion detection mode. For antagonist assay, EC₅₀ determination of the A_{2A} agonist NECA was performed (from 0.05 to 10 000 nM) at fixed concentrations of antagonist.

hA_{2B} Binding Assay (CEREP). A commercial assay (catalog number 801-2bh) was used with human recombinant HEK-293 cells, ligand [³H]-MRS1754 at a final concentration of 0.5 nM ($K_d = 3.75$ nM) and nonspecific ligand NECA (100 μ M) for an incubation of 120 min at 22 °C.

hA₃ Binding Assay from MDS Pharma Services (Now Owned by Ricerca Biosciences, LLC). Commercial assay (catalog number 200720) was used with human recombinant CHO-K1 cells, ligand [³H]-AB-MECA at final concentration of 0.5 nM ($K_d = 5.9$ nM) and nonspecific ligand 1 μ M IB-MECA for an incubation of 60 min at 25 °C.

Data Analysis. The data were fitted with nonlinear regression, and K_i was calculated based on the Cheng–Prusoff equation, $K_i = IC_{50}/(1 - [L]/K_d)$, where [L] is the concentration of the radioligand in the assay and K_d is the dissociation equilibrium constant of the radioligand.

Cytochrome P450 (CYP) Enzyme Inhibition. CYP enzyme inhibition was performed using recombinant enzymes with Supersome, Gentest, expressing individual CYP enzymes (CYP1A2, CYP3A4, CYP2C9, CYP2C19, and CYP2D6). The inhibition of CYP enzymes by the test compounds was assessed by incubating each enzyme with its substrate (7-ethoxy-3-cyanocoumarin was used for CYP1A2 (10 μ M) and CYP2C19 (50 μ M); dibenzylfluorescein (2 μ M) was used for CYP2C9; resorufin benzyl ether (100 μ M) was used for CYP3A4; and 3-[2-(*N,N*-diethyl-*N*-methylamino)ethyl]-7-methoxy-4-methylcoumarin (3 μ M) was used for CYP2D6) alone or in the presence of the test compounds at eight different concentrations (40–0.02 μ M).

All incubations (28 min for CYP1A2, 30 min for CYP3A4, and 45 min for CYP2C9, CYP2C19, and CYP2D6) were performed in phosphate buffer with glucose-6-phosphate dehydrogenase used as cofactor.

At the end of the incubation period, the amount of metabolite formed was measured using a fluorescence spectrophotometer. The excitation and emission wavelengths in nanometers are 450 (ex) and 465 (em) for CYP1A2, CYP2C19, and CYP2D6, 485 (ex) and 535 (em) for CYP2C9, and 530 (ex) and 590 (em) for CYP3A4.

Inhibitions were expressed relative to controls (without inhibitors), and IC₅₀ values were calculated using Microsoft Excel software.

Microsomal Stability Determination. The microsomal intrinsic clearance was determined by assessing the elimination of test compound over the incubation time. The test compounds were incubated at 1 μ M with human and rat microsomes (BD Biosciences) for 60 min, using NADPH as cofactor. An NADPH regenerating system containing NADP⁺, glucose-6-phosphate dehydrogenase, glucose-6-phosphate, sodium citrate, and MgCl₂ (cofactor mix) was used as a source of NADPH. The microsomes were stored at –80 °C, and test tubes with prepared cofactor mix were stored in the freezer until use.

Human and rat microsomes were thawed at room temperature, and cofactor mix was added. The mixture was vortex mixed and put in a water bath at 37 °C for 10 min. The reaction was initiated by adding test compound (final concentration 1 μ M, 0.5 mg of protein/mL).

Separate incubations were made for each test compound and time point. The samples were incubated for 0, 5, 15, 30, and 60 min, and the reactions were stopped by adding 100 μ L of acetonitrile and transferred to a 96 well stop plate with seals. The stop plates were centrifuged for 10 min at 3300 rpm and 4 °C, before being analyzed by liquid-chromatography coupled to a tandem mass spectrometer (LC-MS/MS, Waters QuattroMicro, Manchester, UK).

Hepatocyte Stability Determination. The intrinsic clearances of the test compound in cryopreserved hepatocytes were determined by assessing the disappearance of 0.2 μ M and 1 μ M compound over time by LC/MS-MS. Pooled cryopreserved hepatocytes from humans (three donors), male rats (Sprague–Dawley, two donors), and male dogs (beagle, two donors) from In Vitro Technologies, Inc. Baltimore, MD, USA, were used. Cells were thawed in a 37 °C water bath, and viable cells were suspended in 500 μ L of Dulbecco's modified Eagle medium (high glucose) with 5 mM HEPES buffer in 24 well plates. The cell density used was 10⁶ cells/mL. Incubations were started after 15 min of preincubation, and aliquots (50 μ L) of the cell suspension were transferred to a stop solution (ice-cold acetonitrile) at time points 0, 10, 20, 30, 40, and 60 min after addition of the test compound. The $t_{1/2}$ is scaled to intrinsic clearance values of L/min for humans and mL/min for rats according the method published by Obach et al.⁴⁵ Values of scaling factors are 120 million cells per gram of liver for human and rat and 240 million cells per gram for dog. Liver weight of 45/32/20 g per kg and standard total body weight of 0.25/10/70 kg for rat, dog, and human were used respectively.

Protein Binding. Serum protein binding was determined *in vitro* in rat and human serum following incubation of 0.1 μ M test compound dissolved in PBS in ultracentrifugation filter-plates (300 μ L in each well) (Multiscreen filter plates, 10 kDa MW cutoff, Millipore) for 60 min at 37 °C. Plates were then centrifuged for 60 min at 37 °C (3200 rcf), and the free fraction was measured by LC/MS-MS following addition of internal standard.

Caco-2 Permeability. The polarized transport of the compounds was studied in Caco-2 cells grown on permeable filters (Transwell, Corning Costar) for 21–28 days. For the experiment, a 2 mM DMSO stock solution was diluted to the appropriate concentrations (1–20 μ M) with Hanks–HEPES buffer, pH 7.4. The test solution was added to either the upper chamber (apical-to-basolateral transport, A–B) or the lower chamber (basolateral-to-apical transport, B–A) and from the chamber opposite to the test solution, samples were removed during 240 min and replaced with an equal amount of fresh buffer.

The samples were analyzed by LC-MS/MS (electrospray in positive mode). The apparent permeability coefficient, P_{app} , was calculated as follows:

$$P_{app} = dQ/dt(1/(AC_0))$$

where dQ/dt is the steady-state flux across the monolayer, A is the area of the monolayer (1.1 cm²), and C_0 is the initial concentration in the test solution. A $P_{app,B-A}/P_{app,A-B}$ ratio of one is indicative of pure passive diffusion, whereas a ratio significantly higher than one indicates polarized transport in favor of the B–A direction, suggesting involvement of an efflux system such as P-gp.

In Vivo PK Studies. All dosing vehicles for compound **28** consisted of aqueous 25% cremophore, except suspension studies, where compound **28** was suspended in aqueous 0.5% methylcellulose. The vehicle used for compounds **31** and **32** was aqueous 10% hydroxyl-propyl β -cyclodextrin.

Plasma concentration–time profile of compound **28** was determined from blood samples drawn serially from a catheter implanted in the carotid artery in awake Sprague–Dawley rats. Following administration of test compound, 10 blood samples (100 μ L) were automatically collected (AccuSampler TM, Dilab, Lund, Sweden) over a 20 h period. Bioconversion of the prodrugs **31** and **32** to **28** was assessed in rats using manual blood sampling from the tail vein. Following po administration (2 mL/kg dose volume), six serial blood samples (~100 μ L) were taken from each animal between 5 and 420 min after drug administration.

For brain/plasma exposure studies, cardiac blood was obtained under isoflurane anesthesia. Dose volumes of 5 and 10 mL/kg were applied for rats and mice, respectively. Blood samples were

collected in EDTA-coated tubes and centrifuged for 10 min at 4 °C after which plasma was drawn off. Following decapitation, the brain was removed and stored at -80 °C pending bioanalysis.

PK analysis of the data was performed with PC-compatible software WinNonlin, ver. 4.1 (Pharsight Corporation, Mountain View, CA, USA). A two-compartment model with first-order absorption (po only) and elimination rate was used for PK modeling following administration of compound **28**.⁴⁶ Derived parameters were plasma clearance (CL), volume of distribution at steady-state (V_{ss}), po bioavailability (F), maximum plasma exposure (C_{max}) and time thereto (T_{max}) after po administration, and terminal plasma half-life ($t_{1/2,\beta}$). The concentration–time profiles of compound **28** formed from administration of the prodrugs **31** and **32** were fitted using a one-compartment model. AUCs extrapolated to infinity were applied for calculations of extent of prodrug conversion.

Prediction of Human PK. Prediction of hepatic clearance in humans was done by *in vitro/in vivo* extrapolation from the predicted hepatic clearance in rats and humans and the observed systemic *in vivo* clearance in rats. According to the well-stirred model,³⁰ an approximate hepatic clearance in each species (CL_{pred}) was predicted from hepatocyte intrinsic clearance (CL_{int}) according to

$$CL_{pred} = \frac{LBF \cdot CL_{int} \cdot f_u}{LBF + CL_{int} \cdot f_u}$$

where LBF is liver blood flow and f_u fraction unbound in plasma. Human clearance was then estimated from the observed *in vivo* rat clearance and the *in vitro* clearance prediction in each species ($CL_{pred, human}$; $CL_{pred, rat}$)²⁹ according to

$$CL_{human} = CL_{rat} \frac{CL_{pred, human}}{CL_{pred, rat}}$$

Human volume of distribution at steady-state (V_{ss}) was predicted³¹ according to

$$V_{ss, human} = \frac{f_{u, human}}{f_{u, animal}} V_{ss, animal} + 0.1 \left(1 - \frac{f_{u, human}}{f_{u, animal}} \right)$$

The corresponding predicted effective plasma half-life ($t_{1/2}$) was estimated from the predicted CL and V_{ss} as

$$t_{1/2} = \ln 2 \times V_{ss} / CL$$

Plasma and Brain Bioanalysis. Brain homogenate was prepared by homogenizing the whole brain with 70% acetonitrile (1:4 v/v) followed by centrifugation and collection of the supernatant. Plasma and brain supernatant samples were frozen at -80 °C until analysis. Concentrations of **28** were determined in plasma and brain homogenate using high turbulent flow liquid chromatography (HTLC) (dual column, focus mode, Cohesive Technologies, U.K.) followed by tandem mass spectrometry (MS/MS) detection in positive-ion electrospray ionization mode (Sciex API-3000 MS, Applied Biosystems, the Netherlands). Plasma concentrations of **31** and **32** were determined using inverse-phase high pressure liquid chromatography (HPLC) followed by equivalent MS/MS detection. Samples of plasma and brain homogenate were prepared by adding an equal amount of 10% methanol with internal standard included (escitalopram) and after centrifugation (6000g, 5 °C, 20 min), 10 μ L was injected into the LC/MS/MS system. The mobile phase consisted of water/methanol with 0.1% ammonium hydroxide pumped as a gradient through an XTerra analytical column (MS C8, 2.1 \times 20 mm², Waters Corp., MA, USA). The lower limit of quantification was typically 0.5 ng/mL in plasma and 5 ng/g in brain.

In Vivo Binding Studies. A_{2A} receptor *in vivo* binding was measured as displacement of [³H]SCH58261 (specific activity 60 Ci/mmol) in mouse striatum. Male NMRI mice (18–25 g) were treated po with compound **28** in a dose range from 0.1 to 10 mg/kg. Forty minutes after administration of test substance,

8.5 μ Ci of [³H]SCH58261 on average was injected iv via the tail vein. Ten minutes after iv injection, the animals were sacrificed by cervical dislocation, and the brain was quickly removed. Striatum was dissected out and homogenized in 3.5 mL of ice-cold buffer (50 mM KPO₄, pH 7.4), and 1 mL samples were filtered through Whatman GF/C filters soaked in 0.1% PEI. Filtration was completed within 60 s subsequent to decapitation. Filters were washed 2 times and counted in a liquid scintillation counter, and protein content in the samples was measured using the BCS protein determination assay.⁴⁷ A group of vehicle-treated animals was used to determine total [³H]SCH58261 binding; non-specific binding was determined from radioactivity levels in cerebellum. ED₅₀ value was calculated using nonlinear regression sigmoidal dose–response (variable slope) by Prism (GraphPad Software). Top and bottom of curve were set to 100 and 0, respectively.

Haloperidol-Induced Hypolocomotion. Locomotor activity in male NMRI mice (weighing 20–25 g) was measured using activity boxes equipped with photocells sensitive to infrared light. The activity boxes (20 \times 32 cm²) were equipped with 5 \times 8 infrared light sources and photocells placed 1.8 cm above the floor. The locomotor activity was quantified by counting the number of photobeam interruptions. Recording of an activity count required consecutive interruption of adjacent light beams, thus avoiding counts induced by stationary movements. The mice ($n = 8$ for each group) were dosed po with test substance 30 min before they were injected with 0.63 mg/kg, 10 mL/kg, sc haloperidol. The vehicle for compound **28** was 25% cremophor/isotonic saline, and for haloperidol the vehicle was 0.03% PEG/0.0003% tartaric acid in deionized water. Fifteen minutes later, the mice were placed in locomotor activity boxes. Locomotor activity was measured over the next 20 min. The ED₅₀ value was calculated using nonlinear regression sigmoidal dose–response (variable slope) by Prism (GraphPad Software). Top and bottom of curve were set to 100 and 0, respectively.

Animals. Male NMRI mice and Sprague–Dawley rats were housed in plastic cages in groups of four and were habituated to the animal facilities for at least a week before testing. The temperature (21 \pm 2 °C), relative humidity (55% \pm 5%), and air exchange (16 times per hour) in the housing room were automatically controlled. The animals had free access to commercial food pellets and tap water and were maintained on a 12 h light/dark cycle (0600/1800 h).

Ethical permission for the studies were granted by the animal welfare committee, appointed by the Danish Ministry of Justice, and all animal procedures were carried out in compliance with the EC Directive 86/609/EEC and with the Danish legislation regulating experiments in animals.

Acknowledgment. The authors would like to thank Bitten Hansen, Krestian Larsen, Bente Jensen, Klaus G. Jensen, Mette Larsen, Louise H. Rosendahl, Mette L. Pedersen, Lassina Badolo, Dorrit B Larsen, Mona Elster, Karina J. Kristensen Christina Sveigaard, and Sanne Nielsen for technical assistance.

Supporting Information Available: Preparation and analytical data for compounds **5–30**, hA_{2A} affinity data for compounds **5–9**, **18**, and **19**, results of the broad *in vitro* pharmacology profiling of **28**, and kinetic data for the chemical hydrolysis of **32**. This material is available free of charge via the Internet at <http://pubs.acs.org>.

References

- (1) Fredholm, B.-B.; Abbracchio, M. P.; Burnstock, G.; Daly, J. W.; Harden, T. K.; Jacobson, K. A.; Leff, P.; Williams, M. Nomenclature and classification of purinoceptors. *Pharmacol. Rev.* **1994**, *46*, 143–156.
- (2) Olah, M. E.; Stiles, G. L. The role of receptor structure in determining adenosine receptor activity. *Pharmacol. Ther.* **2000**, *85*, 55–75.

- (3) Xu, K.; Bastia, E.; Schwarzschild, M. Therapeutic potential of adenosine A_{2A} receptor antagonists in Parkinson's disease. *Pharmacol. Ther.* **2005**, *105*, 267–310.
- (4) Simola, N.; Morelli, M.; Pinna, A. Adenosine A_{2A} receptor antagonists and Parkinson's disease: State of the art and future directions. *Curr. Pharm. Des.* **2008**, *14*, 1475–1489.
- (5) Baraldi, P. G.; Tabrizi, M. A.; Gessi, S.; Borea, A. P. Adenosine receptor antagonists: Translating medicinal chemistry and pharmacology into clinical utility. *Chem. Rev.* **2008**, *108*, 238–263.
- (6) Moro, S.; Gao, Z.-G.; Jacobson, K. A.; Spalluto, G. Progress in the pursuit of therapeutic adenosine receptor antagonists. *Med. Res. Rev.* **2006**, *26*, 131–159.
- (7) Yuzlenko, O.; Kić-Kononowicz, K. Potent adenosine A₁ and A_{2A} receptor antagonists: Recent developments. *Curr. Med. Chem.* **2006**, *13*, 3609–3625.
- (8) Sams, A. G.; Mikkelsen, G. K.; Larsen, M.; Torup, L.; Brennum, L. T.; Schröder, T. J.; Bang-Andersen, B. Hit-to-lead optimization of a series of carboxamides of ethyl 2-amino-phenylthiazole-5-carboxylates as novel adenosine A_{2A} receptor antagonists. *Bioorg. Med. Chem. Lett.* **2010**, *20*, 5241–5244.
- (9) Zhang, X.; Tellew, J. E.; Luo, Z.; Moorjani, M.; Lin, E.; Lanier, M. C.; Chen, Y.; Williams, J. P.; Saunders, J.; Lechner, S. M.; Markison, S.; Joswig, T.; Petroski, R.; Piercey, J.; Kargo, W.; Malany, S.; Santos, M.; Gross, R. S.; Wen, J.; Jalali, K.; O'Brien, Z.; Stotz, C. E.; Crespo, M. I.; Dias, J.-L.; Slee, D. H. Lead optimization of 4-acetyl-amino-2-(3,5-dimethylpyrazol-1-yl)-6-pyridylpyrimidines as A_{2A} adenosine receptor antagonists for the treatment of Parkinson's disease. *J. Med. Chem.* **2008**, *51*, 7099–7110.
- (10) Slee, D. H.; Chen, Y.; Zhang, X.; Moorjani, M.; Lanier, M. C.; Lin, E.; Rueter, J. K.; Williams, J. P.; Lechner, S. M.; Markison, S.; Malany, S.; Santos, M.; Gross, R. S.; Jalali, K.; Sai, Y.; Zuo, Z.; Yang, C.; Castro-Palomino, J. C.; Crespo, M. I.; Pratt, R. M.; Dias, J.-L.; Saunders, J. 2-Amino-N-pyrimidin-4-ylacetamides as A_{2A} receptor antagonists: 1. Structure–activity relationships and optimization of heterocyclic substituents. *J. Med. Chem.* **2008**, *51*, 1719–1729.
- (11) Slee, D. H.; Zhang, X.; Moorjani, M.; Klenk, D. C.; Lanier, M. C.; Chen, Y.; Rueter, J. K.; Lechner, S. M.; Markison, S.; Malany, S.; Joswig, T.; Santos, M.; Gross, R. S.; Williams, J. P.; Castro-Palomino, J. C.; Crespo, M. I.; Pratt, R. M.; Gual, S.; Dias, J.-L.; Wen, J.; O'Brien, Z.; Saunders, J. Identification of novel, water-soluble, 2-amino-N-pyrimidin-4-yl acetamides as A_{2A} receptor antagonists with in vivo efficacy. *J. Med. Chem.* **2008**, *51*, 400–406.
- (12) Slee, D. H.; Moorjani, M.; Zhang, X.; Lin, E.; Lanier, M. C.; Chen, Y.; Rueter, J. K.; Lechner, S. M.; Markison, S.; Malany, S.; Joswig, T.; Santos, M.; Gross, R. S.; Williams, J. P.; Castro-Palomino, J. C.; Crespo, M. I.; Pratt, R. M.; Gual, S.; Dias, J.-L.; Jalali, K.; Sai, Y.; Zuo, Z.; Yang, C.; Wen, J.; O'Brien, Z.; Petroski, R.; Saunders, J. 2-Amino-N-pyrimidin-4-ylacetamides as A_{2A} receptor antagonists: 2. Reduction of hERG activity, observed species selectivity, and structure–activity relationships. *J. Med. Chem.* **2008**, *51*, 1730–1739.
- (13) Shao, Y.; Cole, A. G.; Brescia, M.-R.; Qin, L.-Y.; Duo, J.; Stauffer, T. M.; Rokosz, L. L.; McGuinness, B. F.; Henderson, I. Synthesis and SAR studies of trisubstituted purinones as potent and selective adenosine A_{2A} receptor antagonists. *Bioorg. Med. Chem. Lett.* **2009**, *19*, 1399–1402.
- (14) Neustadt, B. R.; Liu, H.; Hao, J.; Greenlee, W. J.; Stamford, A. W.; Foster, C.; Arik, L.; Lachowicz, J.; Zhang, H.; Bertorelli, R.; Fredduzzi, S.; Varty, G.; Cohen-Williams, M.; Ng, K. Potent and selective adenosine A_{2A} receptor antagonists: 1,2,4-triazolo[1,5-c]-pyrimidines. *Bioorg. Med. Chem. Lett.* **2009**, *19*, 967–971.
- (15) Moorjani, M.; Luo, Z.; Lin, E.; Vong, B. G.; Chen, Y.; Zhang, X.; Rueter, J. K.; Gross, R. S.; Lanier, M. C.; Tellew, J. E.; Williams, J. P.; Lechner, S. M.; Malany, S.; Santos, M.; Crespo, M. I.; Dias, J.-L.; Saunders, J.; Slee, D. H. 2,6-Diaryl-4-acylaminopyrimidines as potent and selective adenosine A_{2A} antagonists with improved solubility and metabolic stability. *Bioorg. Med. Chem. Lett.* **2008**, *18*, 5402–5405.
- (16) Mantri, M.; de Graaf, O.; van Veldhoven, J.; Göbliös, A.; von Frijtag Drabbe Künzel, J.; Mulder-Krieger, T.; Link, R.; de Vries, H.; Beukers, M. W.; Brussee, J.; IJzerman, A. P. 2-Amino-6-furan-2-yl-4-substituted nicotinonitriles as A_{2A} adenosine receptor antagonists. *J. Med. Chem.* **2008**, *51*, 4449–4455.
- (17) Lanier, M. C.; Moorjani, M.; Luo, Z.; Chen, Y.; Lin, E.; Tellew, J. E.; Zhang, X.; Williams, J. P.; Gross, R. S.; Lechner, S. M.; Markison, S.; Joswig, T.; Kargo, W.; Piercey, J.; Santos, M.; Malany, S.; Zhao, M.; Petroski, R.; Crespo, M. I.; Dias, J.-L.; Saunders, J.; Wen, J.; O'Brien, Z.; Jalali, K.; Madan, A.; Slee, D. H. N-[6-Amino-2-(heteroaryl)pyrimidin-4-yl]acetamides as A_{2A} receptor antagonists with improved drug like properties and in vivo efficacy. *J. Med. Chem.* **2009**, *52*, 709–717.
- (18) Gillespie, R. J.; Cliffe, I. A.; Dawson, C. E.; Dourish, C. T.; Gaur, S.; Giles, P. R.; Jordan, A. M.; Knight, A. R.; Lawrence, A.; Lerpiniere, J.; Misra, A.; Pratt, R. M.; Todd, R. S.; Upton, R.; Weiss, S. M.; Williamson, D. S. Antagonists of the human adenosine A_{2A} receptor. Part 2: Design and synthesis of 4-arylthieno[3,2-d]pyrimidine derivatives. *Bioorg. Med. Chem. Lett.* **2008**, *18*, 2920–2923.
- (19) Gillespie, R. J.; Bamford, S. J.; Gaur, S.; Jordan, A. M.; Lerpiniere, J.; Mansell, H. L.; Stratton, G. C. Antagonists of the human A_{2A} receptor. Part 5: Highly bio-available pyrimidine-4-carboxamides. *Bioorg. Med. Chem. Lett.* **2009**, *19*, 2664–2667.
- (20) Gillespie, R. J.; Bamford, S. J.; Clay, A.; Gaur, S.; Haymes, T.; Jackson, P. S.; Jordan, A. M.; Klenke, B.; Leonardi, S.; Liu, J.; Mansell, H. L.; Ng, S.; Saadi, M.; Simmonite, H.; Stratton, G. C.; Todd, R. S.; Williamson, D. S.; Yule, I. A. Antagonists of the human A_{2A} receptor. Part 6: Further optimization of pyrimidine-4-carboxamides. *Bioorg. Med. Chem.* **2009**, *17*, 6590–6605.
- (21) Cole, A. G.; Stauffer, T. M.; Rokosz, L. L.; Metzger, A.; Dillard, L. W.; Zeng, W.; Henderson, I. Synthesis of 2-amino-5-benzoyl-4-(2-furyl)thiazoles as adenosine A_{2A} receptor antagonists. *Bioorg. Med. Chem. Lett.* **2009**, *19*, 378–381.
- (22) Jenner, P. Istradefylline, a novel adenosine A_{2A} receptor antagonist, for the treatment of Parkinson's disease. *Expert Opin. Invest. Drugs* **2005**, *14*, 729–738.
- (23) Neustadt, B. R.; Hao, J.; Lindo, N.; Greenlee, W. J.; Stamford, A. W.; Tulshian, D.; Ongini, E.; Hunter, J.; Monopoli, A.; Bertorelli, R.; Foster, C.; Arik, L.; Lachowicz, J.; Ng, K.; Feng, K.-I. Potent, selective, and orally active adenosine A_{2A} receptor antagonists: Arylpiperazine derivatives of pyrazolo[4,3-e]-1,2,4-triazolo[1,5-c]-pyrimidines. *Bioorg. Med. Chem. Lett.* **2006**, *17*, 1376–1380.
- (24) Jaakola, V.-P.; Griffith, M. T.; Hanson, M. A.; Chezerov, V.; Chien, E. Y. T.; Lane, J. R.; IJzerman, A. P.; Stevens, R. C. The 2.6 angstrom crystal structure of a human A_{2A} adenosine receptor bound to an antagonist. *Science* **2008**, *322*, 1211–1217.
- (25) Carlsson, J.; Yoo, L.; Gao, Z.-G.; Irwin, J. J.; Shoishet, B. K.; Jacobson, K. A. Structure-based discovery of A_{2A} adenosine receptor ligands. *J. Med. Chem.* **2010**, *53*, 3748–3755.
- (26) Katritch, V.; Jaakola, V.-P.; Lane, J. R.; Lin, J.; IJzerman, A. P.; Yeager, M.; Kufareva, I.; Stevens, R. C.; Abagyan, R. Structure-based discovery of novel chemotypes for adenosine A_{2A} receptor antagonists. *J. Med. Chem.* **2010**, *53*, 1799–1809.
- (27) *Maestro* v9.0, Schrödinger Inc.: Portland, OR, 2010.
- (28) Higgs, C.; Beuming, T.; Sherman, W. Hydration site thermodynamics explain SARs for thiazolopyrimines analogues binding to the A_{2A} receptor. *ACS Med. Chem. Lett.* **2010**, *1*, 160–164.
- (29) Lave, T.; Coassolo, P.; Reigner, B. Prediction of hepatic metabolic clearance based on interspecies allometric scaling techniques and in vitro-in vivo correlations. *Clin. Pharmacokinet.* **1999**, *36*, 211–231.
- (30) Rowland, M.; Tozer, T. N. *Clinical Pharmacokinetics: Concepts and Applications*; Lippincott, Williams & Wilkins: Philadelphia, PA, 1995.
- (31) McGinnity, D. F.; Collington, J.; Austin, R. P.; Riley, R. J. Evaluation of human pharmacokinetics, therapeutic dose and exposure predictions using marketed oral drugs. *Curr. Drug Metab.* **2007**, *8*, 463–479.
- (32) Mandhane, S. N.; Chopde, C. T.; Ghosh, A. K. Adenosine A₂ receptors modulate haloperidol-induced catalepsy in rats. *Eur. J. Pharmacol.* **1997**, *328*, 135–141.
- (33) Müller, C. E. Prodrug approaches for enhancing the bioavailability of drugs with low solubility. *Chem. Biodiversity* **2009**, *6*, 2071–2083.
- (34) Rautio, J.; Kumpulainen, H.; Heimbach, T.; Olyai, R.; Oh, D.; Järvinen, T.; Savolainen, J. Prodrugs: Design and clinical applications. *Nat. Rev. Drug Discovery* **2008**, *7*, 255–270.
- (35) Stella, V. J.; Nti-Addae, K. W. Prodrug strategies to overcome poor water solubility. *Adv. Drug Delivery Rev.* **2007**, *59*, 677–694.
- (36) Etmeyer, P.; Amidon, G. L.; Clement, B.; Testa, B. Lessons learned from marketed and investigational prodrugs. *J. Med. Chem.* **2004**, *47*, 2393–2404.
- (37) Sauer, R.; Maurinsh, J.; Reith, U.; Fülle, F.; Klotz, K.-N.; Müller, C. E. Water-soluble phosphate prodrugs of 1-propargyl-8-styryl-xanthine derivatives, A_{2A}-selective adenosine receptor antagonists. *J. Med. Chem.* **2000**, *43*, 440–448.
- (38) Gomes, P.; Santos, M. I.; Trigo, M. J.; Castanheiro, R.; Moreira, R. Improved synthesis of amino acid and dipeptide chloromethyl esters using bromochloromethane. *Synth. Commun.* **2003**, *33*, 1683–1693.
- (39) Krise, J. P.; Zygmunt, J.; Georg, G. I.; Stella, V. J. Novel prodrug approach for tertiary amines: Synthesis and preliminary evaluation of *n*-phosphonoxyethyl prodrugs. *J. Med. Chem.* **1999**, *42*, 3094–3100.
- (40) Varia, S.; Stella, V. J. Phenytoin prodrugs V: In vivo evaluation of some water-soluble phenytoin prodrugs in dogs. *J. Pharm. Sci.* **2010**, *73*, 1080–1087.
- (41) Hockemeyer, J.; Burbiel, J. C.; Müller, C. E. Multigram-scale syntheses, stability, and photoreactions of A_{2A} adenosine receptor

- antagonists with 8-styrylxanthine structure: Potential drugs for Parkinson's disease. *J. Org. Chem.* **2004**, *69*, 3308–3318.
- (42) Friesner, R. A.; Murphy, R. B.; Repasky, M. P.; Frye, L. L. Extra precision glide: Docking and scoring incorporating a model of hydrophobic enclosure for protein–ligand complexes. *J. Med. Chem.* **2006**, *49*, 6177–6196.
- (43) MOE version 2009.10. The software is available from the Chemical Computing Group, Inc., 1010 Sherbrooke Street West, Suite 910, Montreal, Quebec, Canada.
- (44) Clark, A. M.; Labute, P. 2D depiction of protein–ligand complexes. *J. Chem. Inf. Model.* **2007**, *47*, 1933–1944.
- (45) Obach, R. S.; Baxter, J. G.; Liston, T. E.; Silber, M.; Jones, B. C.; Macintyre, F.; Rance, D. J.; Wastall, P. The prediction of human pharmacokinetic parameters from preclinical and in vitro metabolism data. *J. Pharm. Exp. Ther.* **1997**, *283*, 46–58.
- (46) Gabrielsson, J.; Weiner, D. *Pharmacokinetic and Pharmacodynamic Data Analysis: Concepts and Applications*; Swedish Pharmaceutical Press: Stockholm, Sweden, 2000.
- (47) Smith, P. K.; Krohn, R. I.; Hermanson, G. T.; Mallia, A. K.; Gartner, F. H.; Provenzano, M. D.; Fujimoto, E. K.; Goeke, N. M.; Olson, B. J.; Klenk, D. C. Measurement of protein using bicinchoninic acid. *Anal. Biochem.* **1985**, *150*, 76–85.